Level anticrossing and related giant optical anisotropy caused by the Stark effect in a strained (110) quantum well

Yasutomo Kajikawa
Optoelectronics Technology Research Laboratory, 5-5 Tohkodai, Tsukuba, Ibaraki 300-26, Japan
(Received 27 October 1993; revised manuscript received 13 December 1993)

The effects of an electric field along the [110] growth axis on the polarization properties of the interband transitions in a (110) quantum well are studied within a multiband effective-mass approximation. The transfer-matrix method is applied to coupled effective-mass equations in order to obtain the eigenenergies and eigenstates of holes under an electric field within a steplike approximation to the potential. The calculated results are shown for a $Ga_xIn_{1-x}As/Al_yIn_{1-y}As$ quantum well grown on a (110) InP substrate in which the $Ga_xIn_{1-x}As$ well layer is strained due to a lattice mismatch to the substrate, while the lattice constant of the $Al_yIn_{1-y}As$ barrier layer is matched to that of the substrate. In the absence of an electric field, the first hole level ($v1$) in a quantum well having a Ga content of $x=0.58$ and a well width of 80 Å is proved to have a light-hole character, while the second level ($v2$) has a heavy-hole character, due to the effect of tensile strain. The calculated result of the electric-field dependence of the hole energy levels for this quantum well shows an anticrossing behavior between the $v1$ and $v2$ levels. The optical matrix element of the dipole transition between the first electron state ($c1$) and the $v1$ or $v2$ state shows an anomalous behavior in the electric-field dependence, related to the anticrossing: For linear polarization along the [110] growth axis, the optical matrix element for the $c1$-$v1$ transition suddenly decreases with increasing field, while that for the $c1$-$v2$ transition rises in the anticrossing region, representing character changes from light- to heavy-hole-like and vice versa; for polarization parallel to the (110) quantum well, the in-plane optical anisotropy is extremely enhanced to as much as 100% near the anticrossing.

I. INTRODUCTION

Until recently, studies on the optical properties of III-V semiconductor quantum wells (QW's) have been mainly restricted to those on (001)-oriented structures.[1] As a matter of course, studies concerning the effects of external fields on QW's have also been restricted to those on (001)-oriented structures.[1] Among the effects of external fields, the effect of an electric field is the most important from the viewpoint of practical applications. The effect of an electric field perpendicular to the QW plane is called the quantum-confined Stark effect (QCSE).[2] Devices based on this effect, such as light modulators, are being intensively studied using (001) QW's.[2]

On the contrary, there are fewer studies concerning the QCSE on differently oriented QW's. Some studies concerning the QCSE on (111) QW's have been published,[3,4] and it has been demonstrated that the shift rate due to the QCSE is larger in a (111) QW than in a (001) QW having the same structure. Regarding (110) QW's, since high-quality QW's have been grown on (110) substrates quite recently,[5–8] only one study has so far been performed regarding the QCSE on (110) QW's.[9] However, the electric-field effect on a (110) QW is quite interesting from both practical and physical viewpoints, as follows.

In a (001) or (111) QW, a hole state at the Brillouin-zone center can be written only with one of the eigenstates of the angular momentum, which corresponds to an eigenvalue of the angular momentum along the growth axis of $J_z=\pm\frac{3}{2}$ or $\pm\frac{1}{2}$, due to the high symmetry of those QW's.[3] The hole state can be classified as either a heavy- or light-hole state according to whether it has an angular momentum of $J_z=\pm\frac{3}{2}$ or $\pm\frac{1}{2}$. When an external field, such as a uniaxial stress, is applied along the growth axis of those QW's, the energy levels of the hole states are shifted while their angular momenta remain unchanged. (This is because the on-axis field does not change the axial symmetry regarding the z axis.) Since the shift rates are different for the hole levels, depending on whether they belong to the heavy- or light-hole state, the energy difference between levels changes with the external field. In some cases, a heavy-hole level and a light-hole level do cross, as shown in Ref. 10 for the on-axis stress, since the two levels belong to different irreducible representations of the point group for the QW system.

On the other hand, if the symmetry of the system (including the experimental configuration for applying the field) is so low that a heavy-hole state and a light-hole state belong to the same irreducible representation, the two hole levels cannot cross each other and show an anticrossing instead. Very recently, such anticrossings between hole levels in QW's or superlattices under low-symmetry configurations have attracted attention.[10–18] These anticrossing behaviors are attracting interest because it has been found that they are accompanied by anomalous changes in the polarization property.

In the case of high-symmetry QW's, such as (001) or (111) QW's, applying an external field along an axis other than the growth axis (an off-axis field) makes the symmetry of the QW system low, enabling anticrossing to be observed. Actually, the anticrossing between hole levels has been shown both theoretically and experimentally for

(001) QW's when a stress or magnetic field is applied along an axis other than the [001] growth axis.[10–14] Among such studies on (001) QW's, Pollak and Qiang[13] as well as Peyla *et al.*[14] reported an anomalous behavior in the polarization property near the anticrossing. Ueno[15] explained the anomalous polarization property of a naturally ordered $Ga_xIn_{1-x}As$ superlattice grown on a (001) InP substrate as being the result of anticrossing between hole levels. This system can also be categorized as an off-axis configuration system, since the $Ga_xIn_{1-x}As$ superlattice is naturally ordered along [111], while the stress due to the lattice mismatch is in the (001) plane.

In QW's oriented other than (001) and (111), not only off-axis fields, but also on-axis fields induce anticrossing to exist, since the symmetry of such QW's is originally low. Some published papers[9,16–18] have dealt with the effects on the on-axis external fields on QW's grown along the low-symmetry axis. The systems described in these papers are a (110) $GaAs/Al_xGa_{1-x}As$ QW under a [110] uniaxial stress,[16] a (311) $GaAs/Al_xGa_{1-x}As$ single heterojunction under a [311] magnetic field,[17,18] and a (110) $Ga_xIn_{1-x}P_yAs_{1-y}$ QW under a [110] electric field.[9]

In the case of an electric field, the on-axis configuration is essentially important, since exciton effects can be seen even under a rather high electric field, as long as the field is along the growth axis.[2] This situation is quite different from the case of applying an in-plane electric field. When the electric field is parallel to the QW plane, excitons are easily dissociated by a low electric field.[2] On the other hand, excitons survive under a rather high electric field along the growth axis, owing to the confinement by the QW potential. Thus, it is much more important to study the effect of an electric field along the growth axis of a low-symmetry QW than to study the effect of an in-plane electric field on a high-symmetry QW.

Moreover, if the ground level (the first level) of holes shows an anticrossing upon applying an electric field, it would be very important from the viewpoint of device applications, since drastic changes in the optical constants are expected at the absorption edge. However, such a situation cannot occur for a QW whose lattice constant is matched to the substrate. In such an unstrained QW, the ground level is heavy-hole-like. The redshift of the heavy-hole level caused by an electric field is larger than that of the light-hole level.[2] Therefore, the difference between the first heavy-hole level and the first light-hole level increases upon applying an electric field. Thus, the two levels never come close.

On the other hand, a light-hole-like level can be the hole ground state in a QW if the QW is subjected to an in-plane tensile stress due to a lattice mismatch to the substrate.[19] In such a strained QW, the ground level of holes is expected to show a slower shift upon applying an electric field than the second hole state which has the heavy-hole character.[20] Therefore, an anticrossing between the first and second hole level is expected upon applying an electric field. Then, one can expect drastic changes in the optical constraints at the absorption edge.

In this paper we consider the effect of an electric field along the growth axis on the polarization property of a (110) QW subjected to tensile strain. In Sec. II, we briefly describe a theoretical model for calculating the energy levels and optical matrix elements within a multiband effective-mass approximation. An efficient analytical method for solving the coupled effective-mass equation has been developed by applying a transfer-matrix method. Details of the calculation method are described in Appendix B. In Sec. III, the calculated results of the energy levels and optical matrix elements are shown for an example of a $Ga_xIn_{1-x}As/Al_yIn_{1-y}As$ QW structure grown on a (110) InP substrate. We first show that the first hole level ($v1$) in the QW has the light-hole character when the Ga content x in $Ga_xIn_{1-x}As$ is sufficiently large to induce a large tensile strain in the well layer. We then show that the $v1$ level in such a strained QW shows an anticrossing with the second hole level ($v2$) upon applying an electric field along the growth axis. Finally, anomalous behaviors of the optical matrix elements for the $c1$-$v1$ and the $c1$-$v2$ transitions are demonstrated.

II. THEORETICAL MODEL

A. Hole eigenstates

In a previous study,[16] we presented an analytical method for obtaining the eigenenergies of holes in a (110) QW under a uniaxial stress along the growth axis, while taking valence-band mixing into account. In the presence of an electric field, however, it becomes much more difficult to obtain the eigenenergies and eigenstates of holes than in the presence of a uniaxial stress or a magnetic field.

In order to obtain the eigenenergies of holes in a low-symmetry QW, such as a (110) QW, within a multiband effective-mass approximation, we must solve a set of coupled effective-mass equations, since valence-band mixing exists even at the Brillouin-zone center. If the potential term in the coupled effective-mass equations is constant in the well and the barrier layer, respectively, an analytical form of the exact solution for the equations can be obtained for each layer.[10,16,21] Since a uniaxial stress or a magnetic field leaves the potential term being constant in each layer, the coupled effective-mass equations have exact analytical solutions, even in the presence of these fields.[10,16,21] On the other hand, an electric field makes the potential term be position dependent. For a single effective-mass equation, an analytical form of the exact solution is still possible even under an inclined potential due to an electric field, using the Airy functions.[2] However, exact analytical solutions are no longer possible for coupled effective-mass equations in the presence of an electric field, and only approximate solutions can be obtained.[22]

One method to obtain an approximate solution for the hole states in a QW under an electric field is to divide a layer into a number of thin sections and to replace the potential with a steplike potential. Since the replaced potential is constant in each section, the coupled effective-mass equations have an analytical form of solution in each section. The problem is then reduced to determining the coefficients in the analytical form so that the boundary conditions at every boundary between the sections are satisfied.

Using the steplike approximation, we deal with a single QW under an electric field, which is grown pseudomorphically on a (110)-oriented substrate. The epitaxial layers are assumed to be strained due to lattice mismatches to the substrate. We take the axes so as to be $x\|[\bar{1}10]$, $y\|[001]$, and $z\|[110]$. The thickness of the well layer is set to be L, and the barrier height is set to be V. We set $z=0$ at the left heterojunction. The electric field along the growth axis z is assumed to be applied only to the well layer. The well layer is equally divided into n sections, and the potential profile of the QW under an electric field is approximated by a steplike potential, as illustrated in Fig. 1. The energy is taken so that the hole energy is positive.

The hole state at the Brillouin-zone center of a (110)-oriented QW can be written as a linear combination between two bases as[16]

$$\Psi_v^{(\pm)}(z)=f_{3/2}(z)u_{\pm 3/2}(z)+f_{1/2}(z)u_{\mp 1/2}(z)\ , \tag{1}$$

where $f_{3/2}(z)$ and $f_{1/2}(z)$ are envelope functions, while $u_{\pm 3/2}(z)$ and $u_{\mp 1/2}(z)$ are the periodic parts of the Bloch functions, which can be written as $u_{\pm 3/2}(z)=|\frac{3}{2},\pm\frac{3}{2}\rangle$ and $u_{\mp 1/2}(z)=|\frac{3}{2},\mp\frac{1}{2}\rangle$. Here, $|J,J_z\rangle$ represents the eigenstate of the angular momentum. The energy levels for $\Psi_v^{(+)}$ and $\Psi_v^{(-)}$ are degenerate.

By setting the "envelope vector" to be a column vector defined by $\mathbf{f}(z)={}^t[f_{3/2}(z),f_{1/2}(z)]$, where the presuperscript t indicates the transpose of a matrix, the effective-mass equations for the hole state in a (110) QW structure can be written as

$$\left[-\frac{\hbar^2}{2m_0}\Gamma_A\frac{d^2}{dz^2}+H_s+U_j\right]\mathbf{f}_j(z)=\varepsilon\mathbf{f}_j(z) \qquad (j=1,\ldots,n) \tag{2a}$$

for the well layer, where the index j denotes the jth section of the well layer which is divided into n sections. For the barrier layers, the effective-mass equations can be written as

$$\left[-\frac{\hbar^2}{2m_0}\Gamma_B\frac{d^2}{dz^2}+H_s+U_j\right]\mathbf{f}_j(z)=(\varepsilon-V)\mathbf{f}_j(z)\ , \tag{2b}$$

with $j=0$ and $n+1$ for the left and right barrier layers, respectively. In each of Eqs. (2a) and (2b), the terms in the square brackets on the left-hand side represent the total Hamiltonian, as a whole. The first term is the kinetic-energy term represented by the Luttinger-Kohn Hamiltonian, the middle term H_S is the strain-energy term represented by the Bir-Pikus Hamiltonian, and the last term U_j is the potential-energy term. The explicit forms of the Luttinger-Kohn and Bir-Pikus Hamiltonians at the zone center in the (110) QW as well as the form of the steplike potential U_j are given in Appendix A. At each boundary of sections, the following current-conserving conditions must be satisfied:

$$\mathbf{f}_j(z_j)=\mathbf{f}_{j+1}(z_j)\ , \tag{3}$$

$$\Gamma_j\mathbf{f}'_j(z_j)=\Gamma_{j+1}\mathbf{f}'_{j+1}(z_j)\ , \tag{4}$$

where $z_j=j\Delta z=j(L/n)$, $\Gamma_j=\Gamma_A$ for $j=1,\ldots,n$, and $\Gamma_j=\Gamma_B$ for $j=0,n+1$. For a bound state, the following conditions at infinity must be satisfied:

$$\mathbf{f}_0(z)=0 \quad (\text{for } z\to-\infty)\ , \tag{5a}$$

$$\mathbf{f}_{n+1}(z)=0 \quad (\text{for } z\to+\infty)\ . \tag{5b}$$

The solutions of effective-mass Eqs. (2a) and (2b) with the boundary conditions defined by Eqs. (3)–(5) give the eigenenergies and eigenstates of holes.

In order to solve a single effective-mass equation with a steplike potential, the transfer-matrix method has been proven to be very useful.[23–31] The transfer-matrix method has also been applied to coupled effective-mass equations by Ram-Mohan, Yoo, and Aggarwal,[32] as well as Valadares,[33] in order to obtain the dispersion curves of holes in a single square-well potential in the absence of an electric field. In the present study, the transfer-matrix method is combined with the analytical method developed in our previous study,[16] in order to obtain the analytical solution for the coupled effective-mass equations under an electric field within a steplike approximation. The method is described in Appendix B.

B. Electron eigenstates and optical matrix elements

The electron state of the conduction band at the zone center of the QW is doubly degenerated, and is written as $\Psi_c^{(\pm)}(z)=f_e(z)u_c^{(\pm)}(z)$, where $f_e(z)$ is an envelope function, while $u_c^{(\pm)}(z)$ is the periodic part of the Bloch function, which can be written as $u_c^{(\pm)}(z)=|\frac{1}{2},\pm\frac{1}{2}\rangle$. The envelope function $f_e(z)$ satisfies an effective-mass equation with a steplike QW potential. The single effective-mass equation for electrons can be solved using an ordinary transfer-matrix method.[23–31]

The optical matrix elements for interband transitions can be calculated using the eigenstates of electrons and holes. We first consider an optical matrix element for circularly polarized light propagating along the z axis. We consider a transition from a conduction-band state which consists of only the $|\frac{1}{2},\frac{1}{2}\rangle$ component. Since the circularly polarized light has an angular-momentum component of $J_z=\pm 1$, the $|\frac{1}{2},\frac{1}{2}\rangle$ state couples with the $|\frac{3}{2},\frac{3}{2}\rangle$ and $|\frac{3}{2},-\frac{1}{2}\rangle$ components of the hole states through circularly polarized light, but does not couple with either the

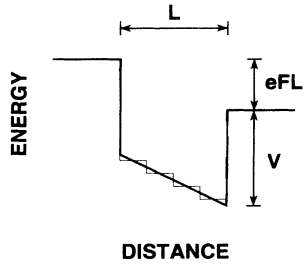

FIG. 1. Quantum-well potential under an electric field and its approximation by a steplike potential.

$|\frac{3}{2},-\frac{3}{2}\rangle$ or $|\frac{3}{2},\frac{1}{2}\rangle$ components, according to the conservation rule for angular momentum. Using the theory of the rotation group, the nonzero elements of the optical matrix elements between the eigenstates of the angular momentum for circular polarization are written as

$$\langle \tfrac{1}{2},\tfrac{1}{2}|\sigma^-|\tfrac{3}{2},\tfrac{3}{2}\rangle=\frac{1}{\sqrt{2}}P \ , \qquad \langle \tfrac{1}{2},\tfrac{1}{2}|\sigma^+|\tfrac{3}{2},-\tfrac{1}{2}\rangle=\frac{1}{\sqrt{6}}P \ , \tag{6}$$

where σ^- and σ^+ represent left- and right-hand-side circular polarization, respectively, and P is the dipole-moment matrix element between orbital "s" and "p" states, i.e., $P=\langle s|p_x|x\rangle=\langle s|p_y|y\rangle=\langle s|p_z|z\rangle$. Note here that P is the same for both the well and the barrier layers, since $|J,J_z\rangle$ are assumed to be the same for the well and barrier layers within the ordinary effective-mass framework.[22] Using the above relations, the optical matrix elements of interband transitions for left- and right-handed circularly polarized light can be written as

$$M_{\rm lhc}=\frac{1}{\sqrt{2}}I_{c3/2}P \ , \qquad M_{\rm rhc}=\frac{1}{\sqrt{6}}I_{c1/2}P \ , \tag{7}$$

where $I_{c3/2}$ and $I_{c1/2}$ are the overlap integrals between the envelope functions, defined as

$$I_{c3/2}=\int_{-\infty}^{+\infty} f_e(z)f_{3/2}(z)dz \ , \qquad I_{c1/2}=\int_{-\infty}^{+\infty} f_e(z)f_{1/2}(z)dz \ . \tag{8}$$

The squared optical matrix elements for the in-plane linear polarization can be calculated from those for circular polarization as

$$|M_x|^2=|M_{\rm lhc}-M_{\rm rhc}|^2=\left|\frac{1}{\sqrt{2}}I_{c3/2}-\frac{1}{\sqrt{6}}I_{c1/2}\right|^2P^2 \ , \qquad |M_y|^2=|M_{\rm lhc}+M_{\rm rhc}|^2=\left|\frac{1}{\sqrt{2}}I_{c3/2}+\frac{1}{\sqrt{6}}I_{c1/2}\right|^2P^2 \ , \tag{9}$$

For π polarization, the selection and intensity rules yield the expression for the nonzero element as

$$\langle \tfrac{1}{2},\tfrac{1}{2}|\pi|\tfrac{3}{2},\tfrac{1}{2}\rangle=(\tfrac{2}{3})^{1/2}P \ . \tag{10}$$

Therefore, the squared optical matrix elements for linear polarization along the growth axis can be calculated as

$$|M_z|^2=\tfrac{2}{3}|I_{c1/2}|^2P^2 \ . \tag{11}$$

It is obvious from Eq. (9) that $|M_x|^2$ or $|M_y|^2$ becomes zero when $I_{c3/2}$ becomes equal to $(1/\sqrt{3})I_{c1/2}$ or $-(1/\sqrt{3})I_{c1/2}$, respectively. In those cases, the transition becomes forbidden for x or y polarization and is allowed only for the y or x component of the in-plane polarization component of light. This occurs whenever two hole states exchange their characters between $|J_z|=\frac{3}{2}$ dominant and $|J_z|=\frac{1}{2}$ dominant, accompanied by an anticrossing of the energy levels, since $|I_{c1/2}/I_{c3/2}|$ varies drastically from a much smaller value to a much larger value than unity, or vice versa, in the anticrossing region.

III. RESULTS OF CALCULATIONS

In this section we present the calculated results of the hole energy levels and the optical matrix elements in a (110) $Ga_xIn_{1-x}As/Al_yIn_{1-y}As$ single QW having a well width of 80 Å. The Al content y in the $Al_yIn_{1-y}As$ barrier layer is chosen to be 0.476, so that the lattice constant of the layer is matched to that of the InP substrate (5.8687 Å). The electron effective mass m_e for $Al_{0.476}In_{0.524}As$ is taken to be $0.074m_0$,[34] while m_e for $Ga_xIn_{1-x}As$ is taken to be $[0.0665x+0.024(1-x)-0.011\,943x(1-x)]m_0$, so that m_e for $Ga_{0.47}In_{0.53}As$ becomes $0.041m_0$.[34] The band-gap energy E_g for $Al_{0.476}In_{0.524}As$ is taken to be 1.511 eV,[34] while E_g for $Ga_xIn_{1-x}As$ is taken to be $(0.4105+0.6337x+0.475x^2)$ eV.[34] The valence-band discontinuity at the (110) heterointerface between $Ga_xIn_{1-x}As$ and $Al_{0.476}In_{0.524}As$ is assumed to be the same as that at the (001) interface between $Ga_{0.47}In_{0.53}As$ and $Al_{0.476}In_{0.524}As$, i.e., 0.196 eV.[34] The validity of the assumption that the valence-band discontinuity is independent of the Ga content is consistent with a theoretical study on band offsets by Anderson and Jones,[35] in which the valence-band discontinuity between $Ga_xIn_{1-x}As$ and InP was calculated to be only slightly dependent on the Ga content. The other parameters used in the calculation are obtained by a linear interpolation between the values for binary semiconductors. The material parameters for AlAs, GaAs, and InAs used in the calculation are listed in Table I. All of the values given in Table I are taken from Ref. 36, except for the Luttinger parameters for GaAs, which are taken from a recent work by Gershoni *et al.*[7]

A. Zero electric field

Figure 2 shows the energy levels of the lowest two states of the hole subbands with even parity at the zone center in the (110) $Ga_xIn_{1-x}As/Al_{0.476}In_{0.524}As$ QW as functions of the Ga content x in the well layer. In Fig. 2, the energies are measured with respect to the valence-band top of bulk $Ga_xIn_{1-x}As$ under the same tensile strain as in the well layer; the hole energy is taken to be positive. Note that the valence-band top of bulk $Ga_xIn_{1-x}As$ subjected to tensile strain is the light-hole band edge and has the $|J_z|=\frac{1}{2}$ dominant character.[19] In unstrained bulk $Ga_xIn_{1-x}As$, the heavy- and light-hole band edges are degenerated. The strain lifts the degeneracy, and the distance between the heavy- and light-hole band edges increases with increasing strain. In Fig. 2, the heavy-hole band edge of strained bulk $Ga_xIn_{1-x}As$, which has the $|J_z|=\frac{3}{2}$ dominant character, is also plotted by a dash-dotted line.

In a (110) QW, the hole states can be classified into the heavy-hole-like or light-hole-like state in the absence of a strain, since the mixing between the bulk heavy-hole Bloch state and light-hole Bloch state is still small.[16] Since the confinement energies are larger for the light-

TABLE I. Material constants used in the calculations.

	Lattice constant (Å)	Luttinger parameters			Stiffness constants (10^{11} dyn/cm^2)			Deformation potentials (eV)		
	a_0	γ_1	γ_2	γ_3	C_{11}	C_{12}	C_{44}	D_d	D_u	D_u'
AlAs	5.660	3.45	0.68	1.29						
GaAs	5.653 25	6.79	1.924	2.782	12.09	5.47	6.03	6.70	2.57	3.94
InAs	6.058 3	19.67	8.37	9.29	8.329	4.526	3.959	5.8	2.7	3.11

hole states than for the heavy-hole states, the first heavy-hole (HH1) state is the ground state of holes. Thus, the first hole level ($v1$) starts from HH1, while the second hole level ($v2$) starts from the first light-hole (LH1) level in the absence of a strain. With increasing Ga content, therefore, the $v1$ level shifts almost parallel to the heavy-hole band edge of $Ga_xIn_{1-x}As$, while the energy of the $v2$ level remains almost unchanged with respect to the valence-band top of strained $Ga_xIn_{1-x}As$ as long as the strain is small. Therefore, the energy difference between the $v1$ and $v2$ levels decreases with increasing Ga content. In the vicinity of a Ga content of 0.565, the two levels come quite close and repel each other. Thus, the $v1$ and $v2$ levels show an anticrossing, as can be seen in Fig. 2.

In the anticrossing region, the two levels exchange their character with each other; after the anticrossing, the $v1$ state has a light-hole character, while the $v2$ level has a heavy-hole character. That is, the strain effect overcomes the confinement effect in the high-strain region beyond the anticrossing.

The character exchange between the $v1$ and $v2$ states is more clearly seen by examining the optical matrix elements for linear polarization along the growth axis, since only the $|J_z|=\frac{1}{2}$ component contributes to $|M_z|^2$, as described by Eq. (11). Figure 3 shows the squared optical matrix elements for z polarization $|M_{[110]}|^2$ for transitions between the first conduction-band state $c1$ and the $v1$ (or $v2$) state at the zone center, as functions of the Ga content x. In the figure the squared matrix elements in the QW are normalized by that for the bulk $Ga_xIn_{1-x}As$, $|M_b|^2=\frac{1}{3}P^2$. It can be clearly seen in Fig. 3 that the $v1$ and $v2$ subbands exchange their character regarding $|J_z|$ with each other when the Ga content passes through $x=0.565$.

Figures 4(a) and 4(b) show the squared optical matrix elements for in-plane polarization $|M_{[\bar{1}10]}|^2$ and $|M_{[001]}|^2$, respectively, for the $c1$-$v1$ and $c1$-$v2$ transitions at the zone center, as functions of the Ga content x. Figure 5 shows the degree of in-plane optical anisotropy

$$P_{\text{in-plane}}=(|M_{[\bar{1}10]}|^2-|M_{[001]}|^2)/(|M_{[\bar{1}10]}|^2+|M_{[001]}|^2)\ ,$$

for those transitions as a function of the Ga content x.

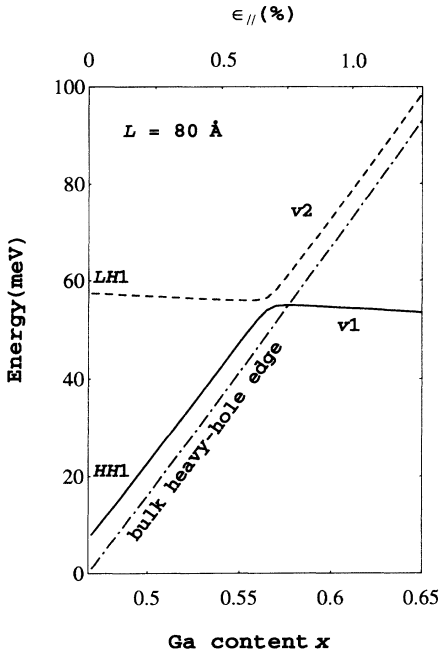

FIG. 2. Energy levels of the lowest two even states ($v1$ and $v2$) of holes at the zone center in a $Ga_xIn_{1-x}As/Al_{0.476}In_{0.524}As$ single-QW structure having a well width of 80 Å grown on a (110) InP substrate as functions of the Ga content x in the $Ga_xIn_{1-x}As$ well layer. The energies are measured with respect to the light-hole band edge of bulk $Ga_xIn_{1-x}As$ under the same strain as in the well layer. The heavy-hole band edge of bulk $Ga_xIn_{1-x}As$ under the same strain is also plotted by a dash-dotted line.

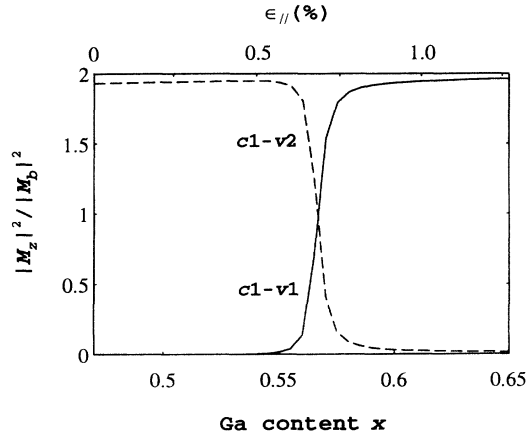

FIG. 3. Squared optical matrix elements of the $c1$-$v1$ (solid line) and the $c1$-$v2$ (dashed line) transitions at the zone center in a $Ga_xIn_{1-x}As/Al_{0.476}In_{0.524}As$ single-QW structure having a well width of 80 Å grown on a (110) InP substrate for linear polarization along the [110] growth axis as functions of the Ga content x in the $Ga_xIn_{1-x}As$ well layer. The values are normalized by the bulk value for $Ga_xIn_{1-x}As$.

The optical matrix elements for x and y polarization show a more complicated behavior than $|M_z|^2$. Especially, $|M_{[\bar{1}10]}|^2$ for the $c1$-$v1$ transition and $|M_{[001]}|^2$ for the $c1$-$v2$ transition vanish at some adequate contents. As a result, the polarization degree $P_{\text{in-plane}}$ becomes 100% at the critical contents. This point has already been discussed in our previous paper.[37] The small difference in the calculated results between the present and previous paper is due to a difference between the finite and infinite barrier height in the models.

Kato, Yu, and Goto[38] studied the intensity of exciton peaks in the absorption spectra of $CuBr_xCl_{1-x}$ as a function of the Br content x. Two absorption peaks, which are called $Z_{1,2}$ and Z_3, were observed in each spectrum of $CuBr_xCl_{1-x}$ in Ref. 38, and the energies of the two exciton peaks showed an anticrossing when they were plotted as a function of the Br content x. Near to the anticrossing, the intensity of the Z_3 exciton peak was observed to completely vanish. The cause of the anticrossing in the case of $CuBr_xCl_{1-x}$ is different from that in the case under consideration in this paper: The anticrossing observed in Ref. 38 is due to exciton-state mixing caused by exchange interaction. Furthermore, the overall intensity of the exciton vanishes in the optically isotropic $CuBr_xCl_{1-x}$ crystal, while the intensity vanishes only for one of the polarization directions in a (110) $Ga_xIn_{1-x}As/Al_yIn_{1-y}As$ QW. In spite of these differences between the two cases, there is a similarity in the two phenomena regarding the point that the intensity vanishes with relevance to an anticrossing in either case. The conduction-band state has a total angular momentum of $J=\frac{1}{2}$ in both cases. The selection and intensity rules for the transition from the state with $J=\frac{1}{2}$ play an important role in both cases.

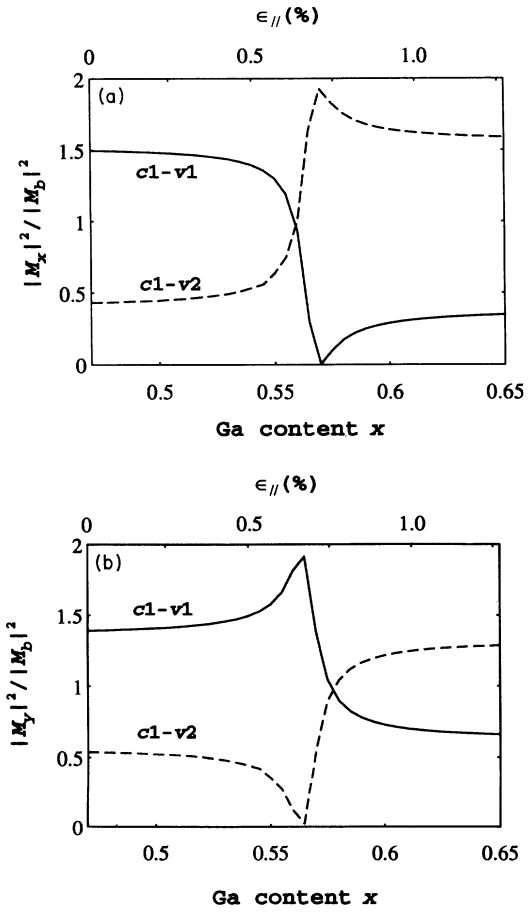

FIG. 4. As in Fig. 3, but for linear polarizations in the (110) QW plane: (a) $[\bar{1}10]$ polarization, (b) [001] polarization.

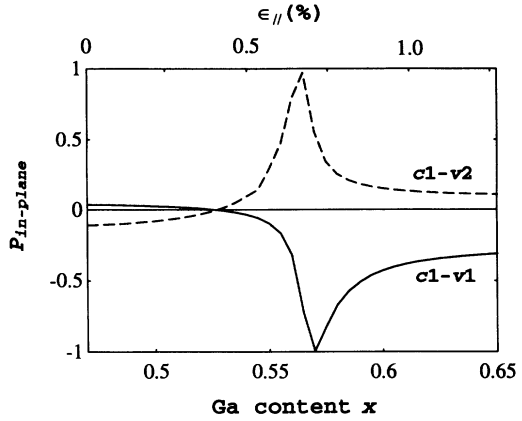

FIG. 5. Degree of in-plane optical anisotropy, $P_{\text{in-plane}}=(|M_{[\bar{1}10]}|^2-|M_{[001]}|^2)/(M_{[\bar{1}10]}|^2+|M_{[001]}|^2)$, for the $c1$-$v1$ (solid line) and $c1$-$v2$ (dashed line) transitions at the zone center in a $Ga_xIn_{1-x}As/Al_{0.476}In_{0.524}As$ single-QW structure having a well width of 80 Å grown on a (110) InP substrate as a function of the Ga content x in the $Ga_xIn_{1-x}As$ well layer.

B. Effect of electric field

As discussed in the previous subsection, the ground state of holes in a (110) $Ga_xIn_{1-x}As/Al_{0.476}In_{0.524}As$ QW having a well width of 80 Å is proven to have the light-hole character when x is larger than 0.57. In such a QW, the first hole level is expected to show a faster shift than the second hole level due to the quantum-confined Stark effect when an electric field is applied. Around an adequate magnitude of the electric field, the $v1$ and $v2$ levels may show an anticrossing behavior. If so, drastic and anomalous changes in the optical matrix elements are expected for the related transitions, as discussed in Sec. II B. In the following, we examine hole energy levels as well as the optical matrix elements in such a QW as a function of the electric field.

We calculated the hole energy levels and the optical matrix elements in a (110) $Ga_xIn_{1-x}As/Al_{0.476}In_{0.524}As$ single QW having a well width of 80 Å as functions of the electric field. The Ga content x in the $Ga_xIn_{1-x}As$ well layer was chosen to be 0.58, so that the $v1$ state has the light-hole character. In the calculation, the well layer is divided into 8 or 16 segments, so that each segment has a width of 10 or 5 Å, respectively. Then the potential is approximated by a steplike potential.

Figure 6 shows the energy levels of the $v1$ and $v2$ states as functions of the electric field F. In Fig. 6, the energies are measured with respect to the valence-band edge of

strained bulk $Ga_{0.58}In_{0.42}As$, as in Fig. 2. In order to see the accuracy of the steplike approximation, the results obtained by dividing the well into 16 segments are compared with those obtained by dividing it into eight segments. For the $v2$ level, the former is represented by a dashed line, while the latter by a dotted line, in Fig. 6. Though the difference between them increases with the electric field, it is only 1 meV at 240 kV/cm. For the $v1$ level, the two results are so close to be undistinguishable in Fig. 6. Thus, the rapid convergence of the steplike approximation is proven for the multiband case, as well as for the one-band case as has been shown in Ref. 30.

In the absence of an electric field, the $v1$ state has the light-hole character while the $v2$ state has the heavy-hole character. Since the redshift due to the QCSE is larger for the heavier confinement mass, the $v2$ level shows a faster shift than the $v1$ level in the small electric-field range. [This situation is similar to the case of the Stark shifts in a (001) $Ga_{0.55}In_{0.45}As/Al_{0.39}In_{0.61}As$ multiple QW calculated by Fritz *et al.*[20]] Thus, the energy difference between the $v1$ and $v2$ levels decreases with increasing electric field. In the vicinity of an electric field of 100 kV/cm, the two levels come quite close and repel each other. Thus, the $v1$ and $v2$ levels show an anticrossing at about $F=100$ kV/cm, as can be seen in Fig. 6.

Figure 7 shows $|M_{[110]}|^2$ for the $c1$-$v1$ and $c1$-$v2$ transitions as functions of the electric field. (The calculated results with the eight-segment approximation and those with the 16-segment approximation were almost undistinguishable also for the matrix elements.) In the figure, the sum of the two squared matrix elements is also plotted by a dash-dotted line. The total of the squared matrix elements shows a moderate quadratic decrease, representing a decrease in the overlap between the electron wave function and the average of the two hole wave functions. The quadratic manner is similar to the intensity decrease often observed for the QCSE in ordinary (001) and (111) QW's.[2,3] However, individual squared matrix elements show more drastic changes: $|M_{[110]}|^2$ for the $c1$-$v1$ transition suddenly decreases in the 70–130 kV/cm range, while that for the $c1$-$v2$ transition raises up in that range, and then gradually decreases. These drastic changes in the optical matrix elements represent character changes between $|J_z|=\frac{3}{2}$ dominant and $|J_z|=\frac{1}{2}$ dominant.

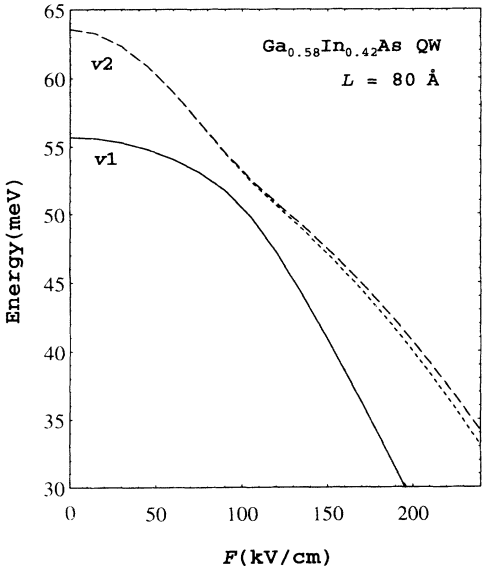

FIG. 6. Energy levels of the lowest two states ($v1$ and $v2$) of holes at the zone center in a $Ga_{0.58}In_{0.42}As/Al_{0.476}In_{0.524}As$ single-QW structure having a well width of 80 Å grown on a (110) InP substrate as functions of the electric field along the [110] growth axis. The energies are measured with respect to the valence-band edge of bulk $Ga_{0.58}In_{0.42}As$ under the same strain as in the well layer. For the $v2$ state, the results obtained in the eight-segment approximation are represented by a dotted line, while those obtained in the 16-segment approximation by a dashed line.

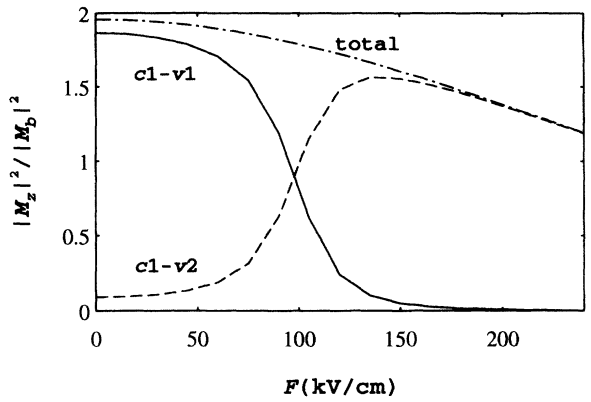

FIG. 7. Squared optical matrix elements of the $c1$-$v1$ (solid line) and the $c1$-$v2$ (dashed line) transitions at the zone center in a $Ga_{0.58}In_{0.42}As/Al_{0.476}In_{0.524}As$ single-QW structure having a well width of 80 Å grown on a (110) InP substrate for linear polarization along the [110] growth axis as functions of the electric field along [110]. The sum of the two squared optical matrix elements is also plotted by dash-dotted line. The values are normalized by the bulk value for $Ga_{0.58}In_{0.42}As$.

Figures 8(a) and 8(b) show squared optical matrix elements for the in-plane polarization $|M_{[\bar{1}10]}|^2$ and $|M_{[001]}|^2$, respectively, for the $c1$-$v1$ and $c1$-$v2$ transitions as functions of the electric field. Figure 9 shows the degree of in-plane anisotropy $P_{\text{in-plane}}$ for the $c1$-$v1$ and $c1$-$v2$ transitions as a function of the electric field. The behaviors of the anisotropy degrees shown in Fig. 9 when the electric field is increased are just similar to those in Fig. 5 when the Ga content x is decreased from $x=0.58$. As the electric field is increased, the anisotropy degrees for the $c1$-$v1$ and $c1$-$v2$ transitions increase, reach a maximum of 100%, and then decrease. The maximum is reached at about $F=90$ kV/cm for the $c1$-$v1$ transition, while $F=105$ kV/cm for the $c1$-$v2$ transition. It has thus been shown that a complete linear polarization of 100% can be seen in the in-plane polarization of a (110) QW when an electric field is applied along the growth axis, while the complete linear polarization has been shown when an external [110] uniaxial stress is applied in our previous paper.[16]

In order to observe the above-mentioned field effect experimentally, one may need a very high-quality sample. The drastic changes in optical matrix elements occur where the two valence-band levels are closest together energetically, and the separation is only a few meV at that time. Therefore, samples with exciton linewidths less

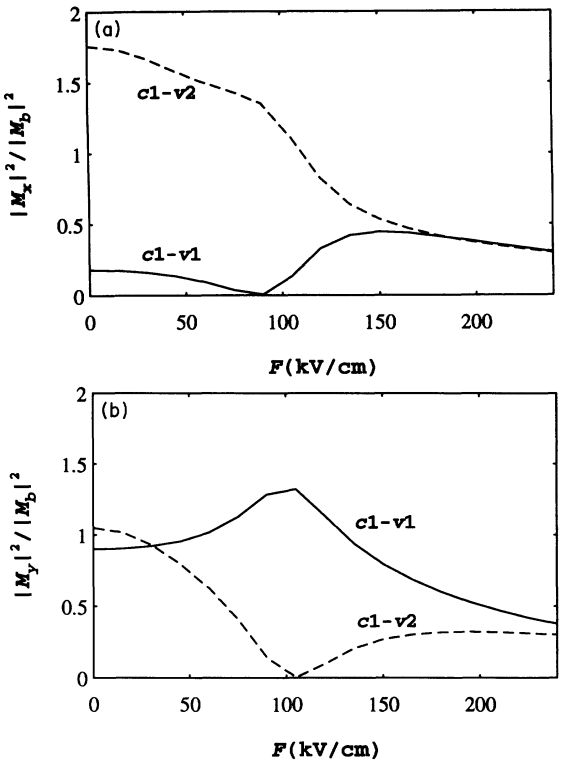

FIG. 8. As in Fig. 7, but for linear polarizations in the (110) QW plane: (a) for [$\bar{1}$10] polarization, (b) for [001] polarization.

than 2 meV are preferable. Since such narrow linewidths have been realized for (001) and (111) quantum wells,[39] the author believes that the narrow linewidth will be realized also for (110) quantum wells.

Oe *et al.*[9] experimentally studied the QCSE of $Ga_xIn_{1-x}As_yP_{1-y}$ QW's grown on (110) InP substrates, using photocurrent spectroscopy. The well layers in the QW structures studied there were compressively strained, however. In such compressively strained QW's, the energy difference between the $v1$ and $v2$ levels increases upon applying an electric field. Therefore, the phenomena related to the anticrossing of hole levels cannot be observed in their QW's. Instead, Oe *et al.* observed another

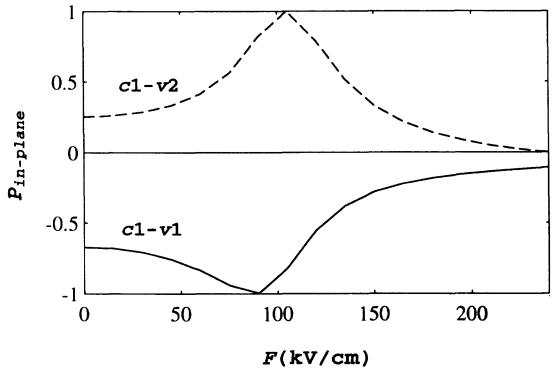

FIG. 9. Degree of in-plane optical anisotropy, $P_{\text{in-plane}}=(|M_{[\bar{1}10]}|^2-|M_{[001]}|^2)/(|M_{[\bar{1}10]}|^2+|M_{[001]}|^2)$, for the $c1$-$v1$ (solid line) and $c1$-$v2$ (dashed line) transitions at the zone center in a $Ga_{0.58}In_{0.42}As/Al_{0.476}In_{0.524}As$ single-QW structure having a well width of 80 Å grown on a (110) InP substrate as a function of the electric field along the [110] growth axis.

strange phenomenon. The absorption current due to the excitonic transition associated with the $v1$ level was enhanced with increasing applied voltage for [001] polarized light, while it was not for [$\bar{1}$ 10] polarized light. We cannot find any explanation for this phenomenon within the framework of the present study.

Citrin and Chang[40] calculated the optical matrix elements in a coupled wire array as a function of an electric field applied perpendicularly to the quantum wire. They found that drastic changes in the optical matrix elements emerge when the related hole level in the quantum wire shows an anticrossing with another hole level. This anticrossing is due to a lowered symmetry due to a two-dimensional confinement by the quantum-wire structure. On the other hand, we have shown in this paper that the anticrossing-related drastic changes in the optical matrix elements can be observed even when the confinement is one-dimensional if the symmetry of the QW is low.

The electropleochroism effect described in this paper can be regarded as being a giant Kerr effect in a QW: a quantum-well Kerr effect. At the same time, it can be regarded as being one of special examples of a field-induced anomalous pleochroism which is widely observed in semiconductor structures under external fields with low-symmetry configurations, including both on- and off-axis cases.

IV. CONCLUSIONS

An efficient analytical method was developed for solving coupled effective-mass equations with a steplike potential by extending a transfer-matrix method for a single effective-mass equation. This newly developed method was applied to the calculation of energy levels, wave functions, and optical matrix elements at the zone center of a lattice-mismatched (110) QW under an electric field along the [110] growth axis. The calculated results of the electric-field dependence of the energy levels clearly showed an anticrossing between the first two hole subbands. Furthermore, it has been shown that the hole-level anticrossing is accompanied by drastic changes in the optical matrix elements. For linear polarization along the [110] growth axis, the optical matrix element for the $c1$-$v1$ transition suddenly decreases upon increasing the field, while that for the $c1$-$v2$ transition rises up in the anticrossing region, representing character changes from light- to heavy-hole-like and vice versa. For polarization parallel to the (110) quantum well, in-plane optical anisotropy is extremely enhanced to be as much as 100% near the anticrossing.

Thus, an anomaly in the in-plane optical anisotropy related to the hole-level anticrossing has been demonstrated in the present study for anticrossing induced by an electric field, while it had been demonstrated for the anticrossing induced by a uniaxial stress in our previous study.[16] We will also demonstrate the anomaly for the anticrossing induced by the magnetic field in our coming study.

ACKNOWLEDGMENTS

The author would like to thank Dr. Yoshifumi Katayama for continuous encouragement. The author also

thanks Professor Kenji Nakao of University of Tsukuba for his critical reading of the manuscript.

APPENDIX A: EXPLICIT FORM OF THE HAMILTONIAN

The expression of the Luttinger-Kohn Hamiltonian in coordinates with z parallel to [110] can easily be obtained from the expression in ordinary coordinates with $z\|[001]$ by a conventional coordinate transformation.[41,42] In coordinates with $z\|[110]$, the 4×4 matrix form of the Luttinger-Kohn Hamiltonian becomes block-diagonal at the Brillouin-zone center of a (110)-oriented QW, where $k_x=k_y=0$. The 2×2 block of the Luttinger-Kohn Hamiltonian H_K for the basis set of $\{u_{3/2},u_{-1/2}\}$ or $\{u_{-3/2},u_{1/2}\}$ can be written as follows:[37]

$$H_K=-\frac{\hbar^2}{2m_0}\Gamma\frac{d^2}{dz^2}\ . \tag{A1}$$

Above, the 2×2 matrix Γ is defined as

$$\Gamma=\gamma_1 I+\begin{bmatrix}-\gamma_a & \gamma_c\\ \gamma_c & \gamma_a\end{bmatrix}\ , \tag{A2}$$

with

$$\gamma_a=\tfrac{1}{2}\gamma_2+\tfrac{3}{2}\gamma_3\ , \tag{A3a}$$

$$\gamma_c=(\sqrt{3}/2)(\gamma_3-\gamma_2)\ , \tag{A3b}$$

where γ_1, γ_2, and γ_3 are Luttinger parameters, and I is the 2×2 unit matrix.

The expression of the Bir-Pikus strain-energy Hamiltonian in coordinates with $z\|[110]$ is obtained in a similar manner as in the above. In this coordinate system, 4×4 matrix form of the Bir-Pikus Hamiltonian for a strained layer grown on a (110)-oriented substrate also has the block diagonal form. The 2×2 block of the Bir-Pikus Hamiltonian can be written as[37]

$$H_S=-\sigma I-\begin{bmatrix}-\xi & \eta\\ \eta & \xi\end{bmatrix}\ , \tag{A4}$$

with

$$\sigma=D_d(3\epsilon_\|-\Delta\epsilon)\ ,\quad \xi=(\tfrac{1}{6}D_u+\tfrac{1}{2}D_u')\Delta\epsilon\ , \tag{A5}$$

$$\eta=\frac{1}{2\sqrt{3}}(D_u'-D_u)\Delta\epsilon\ ,\quad \Delta\epsilon=\frac{2(C_{11}+2C_{12})}{C_{11}+C_{12}+2C_{44}}\epsilon_\|\ ,$$

where D_d, D_u, and D_u' are deformation potentials, and the C's are stiffness constants. The in-plane strain $\epsilon_\|=\epsilon_{xx}=\epsilon_{yy}$ is defined as $\epsilon_\|=(a_0^{\rm epi}-a_0^{\rm sub})/a_0^{\rm epi}$, where $a_0^{\rm epi}$ and $a_0^{\rm sub}$ are the lattice constants of materials comprising the epitaxial layer and the substrate, respectively.

The potential term U_j is represented by a steplike potential:

$$U_j=eF\left[j-\frac{1}{2}-\frac{n}{2}\right]\Delta z\quad (j=0,\ldots,n+1) \tag{A6}$$

APPENDIX B: AN ANALYTICAL METHOD FOR SOLVING COUPLED EFFECTIVE-MASS EQUATIONS WITH A STEPLIKE POTENTIAL UTILIZING THE TRANSFER MATRIX

In this Appendix, we present an effective analytical method for solving coupled effective-mass equations with steplike potential terms. First, coupled effective-mass equations are transformed to a set of uncoupled effective-mass equations. Next, the transformed equations with boundary conditions are solved utilizing the transfer matrix. Finally, a secular equation for determining the eigenenergies is presented.

1. Decoupling of effective-mass equations and the general form of solutions

Coupled effective-mass Eqs. (2a) and (2b) can be decoupled as follows. First, we rewrite Eqs. (2a) and (2b) as

$$\frac{d^2}{dz^2}\mathbf{f}_j(z)=-D_j\mathbf{f}_j(z)\ , \tag{B1}$$

where

$$D_j=\frac{2m_0}{\hbar^2}\Gamma_A^{-1}(\varepsilon I-H_s-U_j)\quad (j=1,\ldots,n)\ , \tag{B2a}$$

$$D_j=\frac{2m_0}{\hbar^2}\Gamma_B^{-1}(\varepsilon I-H_s-U_j-V)\quad (j=0,n+1)\ . \tag{B2b}$$

Let the matrix T_j be the transformation matrix which diagonalizes D_j such that

$$T_j^{-1}D_jT_j=K_j^2\ , \tag{B3}$$

where K_j is a diagonal matrix written as

$$K_j=\begin{bmatrix}k_{j(+)} & 0\\ 0 & k_{j(-)}\end{bmatrix}\ . \tag{B4}$$

We define the transformed envelope vector $\mathbf{g}_j$ as a column vector transformed from $\mathbf{f}_j$ by T_j^{-1}:

$$\mathbf{g}_j(z)=T_j^{-1}\mathbf{f}_j(z)=\begin{bmatrix}g_{j(+)}(z)\\ g_{j(-)}(z)\end{bmatrix}\ . \tag{B5}$$

Then, the derivative equations for $\mathbf{g}_j$ become uncoupled,

$$\frac{d^2}{dz^2}g_{j(+)}(z)=-k_{j(+)}^2g_{j(+)}(z)\ , \tag{B6a}$$

$$\frac{d^2}{dz^2}g_{j(-)}(z)=-k_{j(-)}^2g_{j(-)}(z)\ . \tag{B6b}$$

The general form of the solutions for Eqs. (B6a) and (B6b) can be written as

$$\mathbf{g}_j(z)=\exp(iK_jz)\mathbf{a}_j+\exp(-iK_jz)\mathbf{b}_j\ , \tag{B7}$$

where $\mathbf{a}_j$ and $\mathbf{b}_j$ are constant column vectors. For a bound state,

$$iK_0=\tilde{K}_0=\begin{bmatrix}\kappa_{0(+)} & 0\\ 0 & \kappa_{0(-)}\end{bmatrix}\ ,\quad \mathbf{b}_0=\mathbf{0} \tag{B8a}$$

and

$$iK_{n+1}=\tilde{K}_{n+1}=\begin{bmatrix}\kappa_{n+1(+)} & 0\\ 0 & \kappa_{n+1(-)}\end{bmatrix}, \quad \mathbf{a}_{n+1}=\mathbf{0} \tag{B8b}$$

must be satisfied for $\mathbf{g}_0(z)$ and $\mathbf{g}_{n+1}(z)$, respectively, where the κ's are positive real numbers.

The transformed current-conserving conditions are written as

$$T_j\mathbf{g}_j(z_j)=T_{j+1}\mathbf{g}_{j+1}(z_j)\ , \tag{B9a}$$

$$\Gamma_j T_j\mathbf{g}'_j(z_j)=\Gamma_{j+1}T_{j+1}\mathbf{g}'_{j+1}(z_j)\ . \tag{B9b}$$

2. Transfer-matrix normalism

In order to solve Eqs. (B6a) and (B6b) under boundary conditions (B9a) and (B9b), we set

$$\underline{\mathbf{G}}_j(z)=\begin{bmatrix}\mathbf{g}_j(z)\\ \mathbf{g}'_j(z)\end{bmatrix}\ . \tag{B10}$$

The general form of $\underline{\mathbf{G}}_j(z)$ can be written as

$$\underline{\mathbf{G}}_j(z)=\underline{\Theta}_j(z)\underline{\mathbf{A}}_j\ , \tag{B11}$$

where

$$\underline{\mathbf{A}}_j=\begin{bmatrix}\mathbf{a}_j\\ \mathbf{b}_j\end{bmatrix} \tag{B12}$$

and

$$\underline{\Theta}_j(z)=\begin{bmatrix}\exp(iK_jz) & \exp(-iK_jz)\\ iK_j\exp(iK_jz) & -iK_j\exp(-iK_jz)\end{bmatrix}\ . \tag{B13}$$

The matrix formulation of the current-conserving condition can be written as

$$\underline{T}_j\underline{\mathbf{G}}_j(z_j)=\underline{T}_{j+1}\underline{\mathbf{G}}_{j+1}(z_j)\ , \tag{B14}$$

where

$$\underline{T}_j=\begin{bmatrix}T_j & 0\\ 0 & \Gamma_jT_j\end{bmatrix}\ . \tag{B15}$$

The transfer matrix is defined as

$$\underline{M}_j=\underline{\Theta}_j(z_j)\underline{\Theta}_j(z_{j-1})^{-1}=\begin{bmatrix}\cos(K_j\Delta z) & K_j^{-1}\sin(K_j\Delta z)\\ -K_j\sin(K_j\Delta z) & \cos(K_j\Delta z)\end{bmatrix}\ . \tag{B16}$$

The transfer matrix $\underline{M}_j$ relates the values of $\underline{\mathbf{G}}_j(z)$ at the both ends of the jth section as

$$\underline{\mathbf{G}}_j(z_j)=\underline{M}_j\underline{\mathbf{G}}_j(z_{j-1})\ . \tag{B17}$$

By inserting Eq. (B17) into Eq. (B14), we obtain

$$\underline{R}_j\underline{\mathbf{G}}_{j+1}(z_j)=\underline{M}_j\underline{\mathbf{G}}_j(z_{j-1})\ , \tag{B18}$$

where we have set $\underline{R}_j=\underline{T}_j^{-1}\underline{T}_{j+1}$. By repeating the application of Eq. (B18), we obtain

$$\underline{\mathbf{G}}_n(z_{n-1})=\underline{S}_{n-1}\cdots\underline{S}_1\underline{\mathbf{G}}_1(z_0)\ , \tag{B19}$$

where $\underline{S}_j=\underline{R}_j^{-1}\underline{M}_j$. By setting $\underline{Q}=\underline{M}_n\underline{S}_{n-1}\cdots\underline{S}_1$, together with using Eq. (B17) for $j=n$, we obtain

$$\underline{\mathbf{G}}_n(z_n)=\underline{Q}\underline{\mathbf{G}}_1(z_0) \tag{B20}$$

as the relation of the values of $\underline{\mathbf{G}}(z)$ at both ends of the well. This expression is useful for an infinitely-high-barrier model. For a useful expression in a finite-barrier-height model, we obtain

$$\underline{\mathbf{G}}_{n+1}(z_n)=\underline{W}\underline{\mathbf{G}}_0(z_0)\ , \tag{B21}$$

where

$$\underline{W}=\underline{R}_n^{-1}\underline{Q}\underline{R}_0^{-1}=\begin{bmatrix}W_{AA} & W_{AB}\\ W_{BA} & W_{BB}\end{bmatrix}\ . \tag{B22}$$

3. Solution for bound states

For a bound state, using the conditions of Eqs. (B8a) and (B8b) for $\mathbf{g}_0(z)$ and $\mathbf{g}_{n+1}(z)$, Eq. (B21) is written explicitly as

$$\begin{bmatrix}\exp(-\tilde{K}_{n+1}L)\mathbf{b}_{n+1}\\ -\tilde{K}_{n+1}\exp(-\tilde{K}_{n+1}L)\mathbf{b}_{n+1}\end{bmatrix}=\begin{bmatrix}W_{AA} & W_{AB}\\ W_{BA} & W_{BB}\end{bmatrix}\begin{bmatrix}\mathbf{a}_0\\ \tilde{K}_0\mathbf{a}_0\end{bmatrix}\ . \tag{B23}$$

Removal of $\mathbf{b}_{n+1}$ from Eq. (B23) yields

$$[\tilde{K}_{n+1}(W_{AA}+W_{AB}\tilde{K}_0)+(W_{BA}+W_{BB}\tilde{K}_0)]\mathbf{a}_0=\mathbf{0}\ . \tag{B24}$$

In order that Eq. (B24) has a nontrivial solution, the corresponding secular equation,

$$\det|W_{AA}+W_{AB}\tilde{K}_0+\tilde{K}_{n+1}^{-1}W_{BA}+\tilde{K}_{n+1}^{-1}W_{BB}\tilde{K}_0|=0\ , \tag{B25}$$

must be satisfied. Secular equation (B25) determines the eigenenergies. Then, Eq. (B24) determines the coefficients in the wave function of a bound state together with the normalization condition.

[1]See, for example, G. Bastard, *Wave Mechanics Applied to Semiconductor Heterostructures* (Les Éditions de Physique, Les Ulis, 1990), Chaps. VII and VIII.

[2]D. A. B. Miller, D. S. Chemla, T. C. Damen, A. C. Gossard, W. Wiegmann, T. H. Wood, and C. A. Burrus, Phys. Rev. B **32**, 1043 (1985).

[3]Y. Kajikawa, N. Sugiyama, T. Kamijoh, and Y. Katayama, Jpn. J. Appl. Phys. **28**, L1022 (1989); Y. Kajikawa, M. Hata, N. Sugiyama, and Y. Katayama, Phys. Rev. B **42**, 9540 (1990).

[4]S. M. Shank and G. W. Wicks, J. Cryst. Growth **111**, 440 (1991).

[5]Y. Kajikawa, M. Hata, T. Isu, and Y. Katayama, Surf. Sci. **267**, 501 (1992).

[6]G. Tanaka, K. Hirakawa, H. Ichinose, and T. Ikoma, in *GaAs and Related Compounds,* edited by G. B. Stringfellow, IOP Conf. Proc. No. 120 (Institute of Physics, Bristol, U.K., 1992), p. 25.

[7]D. Gershoni, I. Brener, G. A. Baraff, S. N. G. Chu, L. N. Pfeiffer, and K. West, in *GaAs and Related Compounds* (Ref. 6), p. 419.

[8]R. Bhat, M. A. Koza, D. M. Hwang, M. J. S. P. Brasil, R. E. Nahory, and K. Oe, J. Cryst. Growth **124**, 311 (1992).

[9]K. Oe, K. Wakita, R. Bhat, and M. A. Koza, in *Proceedings of Integrated Photonics Research, New Orleans,* Vol. 10, OSA Technical Digest Series (Optical Society of America, Washington, DC, 1992), p. 18; Electron. Lett. **28**, 1390 (1992).

[10]J. Lee, C. Jagannath, M. O. Vassel, and E. S. Koteles, Phys. Rev. B **37**, 4164 (1988).

[11]M. B. Stanaway, C. J. G. M. Langerak, R. A. J. Thomeer, J. M. Chamberlain, J. Singleton, M. Henini, O. H. Hughes, A. J. Page, and G. Hill, Semicond. Sci. Technol. **6**, 208 (1991).

[12]P. Boring, J.-M. Jancu, B. Gil, D. Bertho, C. Jouanin, and K. J. Moore, Phys. Rev. B **46**, 4764 (1992).

[13]F. H. Pollak and H. Qiang, Jpn. J. Appl. Phys. Suppl. **32-1**, 101 (1993).

[14]P. Peyla, A. Wasiela, Y. Merle d'Aubigné, D. E. Ashenford, and B. Lunn, Phys. Rev. B **47**, 3783 (1993).

[15]Y. Ueno, Appl. Phys. Lett. **62**, 553 (1993).

[16]Y. Kajikawa, Phys. Rev. B **47**, 3649 (1939); Jpn. J. Appl. Phys. Suppl. **32-1**, 101 (1993).

[17]K. Hirakawa, Y. Zhao, M. B. Santos, M. Shayegen, and D. C. Tsui, Phys. Rev. B **47**, 4076 (1993).

[18]S. J. Hawksworth, S. Hill, T. J. B. M. Janssen, J. M. Chamberlain, J. Singleton, U. Ekenberg, G. M. Summers, G. A. Davies, R. J. Nicholas, E. V. Valadares, M. Henini, and J. A. A. J. Perenboom, Semicond. Sci. Technol. **8**, 1465 (1993).

[19]See, for example, J. Y. Marzin, in *Heterojunctions and Semiconductor Superlattices,* edited by G. Allan, G. Bastard, N. Boccara, M. Lannoo, and M. Voos (Springer-Verlag, Berlin, 1986), p. 161.

[20]I. J. Fritz, J. F. Klem, T. M. Brennan, J. R. Wendt, and T. E. Zipperian, Superlatt. Microstruct. **10**, 99 (1991).

[21]L. C. Andreani, A. Psquarello, and F. Bassani, Phys. Rev. B **36**, 5887 (1987).

[22]G. Bastard, *Wave Mechanics Applied to Semiconductor Heterostructures* (Ref. 1), Chap. III.

[23]R. Tsu and L. Esaki, Appl. Phys. Lett. **22**, 562 (1973).

[24]M. Ya. Azbel, Phys. Rev. B **28**, 4106 (1983).

[25]B. Ricco and M. Ya. Azbel, Phys. Rev. B **29**, 1970 (1984).

[26]M. O. Vassell, J. Lee, and H. F. Lockwood, J. Appl. Phys. **54**, 5206 (1983).

[27]R. M. Kolbas and N. Holonyak, Jr., Am. J. Phys. **52**, 431 (1984).

[28]M. J. Kelley, Electron. Lett. **20**, 771 (1984).

[29]A. Harwit, J. S. Harris, Jr., and A. Kapitulnik, J. Appl. Phys. **60**, 3211 (1986).

[30]E. E. Mendez, in *Proceedings of a NATO Advanced Study Institute on Physics and Applications of Quantum Wells and Superlattices,* edited by E. E. Mendez and K. von Klitzing (Plenum, New York, 1987), p. 159.

[31]L. Viña, E. E. Mendez, W. I. Wang, L. L. Chang, and L. Esaki, J. Phys. C **20**, 2803 (1987).

[32]L. R. Ram-Mohan, K. H. Yoo, and R. L. Aggarwal, Phys. Rev. B **38**, 6151 (1988).

[33]E. V. Valadares, Phys. Rev. B **46**, 3935 (1992).

[34]J. Böhrer, A. Krost, T. Wolf, and D. Bimberg, Phys. Rev. B **47**, 6439 (1993).

[35]N. G. Anderson and S. D. Jones, J. Appl. Phys. **70**, 4342 (1991).

[36]D. Bimberg, in *Physics of Group IV Elements and III-V Compounds,* edited by O. Madelung, Landolt-Börnstein, New Series, Group III, Vol. 17, Pt. A (Springer-Verlag, Berlin, 1982).

[37]Y. Kajikawa and M. Hata, Superlatt. Microstruct. **12**, 355 (1992).

[38]Y. Kato, C. I. Yu, and T. Goto, J. Phys. Soc. Jpn. **28**, 104 (1970).

[39]Y. Kajikawa, Phys. Rev. B **48**, 7935 (1993).

[40]D. S. Citrin and Y.-C. Chang, Appl. Phys. Lett. **59**, 582 (1991).

[41]G. E. W. Bauer, in *Spectroscopy of Semiconductor Microstructures,* edited by G. Fasol, A. Fasolino, and P. Lugli (Plenum, New York, 1989), p. 381.

[42]J. B. Xia, Phys. Rev. B **43**, 9856 (1991).